Polímeros
ISSN 1678-5169 (Online)

https://doi.org/10.1590/0104-1428.08220

ORIGINAL ARTICLE

Melt-mixed nanocomposites of SIS/MWCNT: rheological, electrical and structural behavior

Ludimilla Barbosa Ferreira[1], Rayane de Souza Fernandes[1], Rosario Elida Suman Bretas[2] and João Paulo Ferreira Santos[1]*

[1]Departamento de Engenharia de Materiais – DEMAT, Centro Federal de Educação Tecnológica de Minas Gerais – CEFET-MG, Belo Horizonte, MG, Brasil

[2]Departamento de Engenharia de Materiais – DEMa, Universidade Federal de São Carlos – UFSCar, São Carlos, SP, Brasil

**joaopaulofsbrasil@gmail.com*

Abstract

In this work, nanocomposites based on the triblock copolymer polystyrene-b-polyisoprene-b-polystyrene (SIS) thermoplastic elastomer filled with multiwall carbon nanotubes (MWCNT) were obtained by melt mixing. The nanocomposites were characterized by oscillatory rheometry, electrical resistivity, small angle x-ray scattering (SAXS) and transmission electron microscopy (TEM). The results showed that both, rheological and electrical percolation were achieved at MWCNT loadings between 1-3 vol.%. Rheological tests revealed that the insertion of MWCNT into SIS significantly enhanced the process of relaxation of SIS blocks. Resistivity measurements revealed that conductive nanocomposites were obtained at MWCNT loadings ~1.6 vol.%. The electrical resistivity decreased eleven orders of magnitude from neat SIS to SIS/ 5 vol.% MWCNT. Finally, SAXS and TEM showed that the melt mixing process and the presence of MWCNT hampered the self-assembly of SIS into well-ordered domains.

Keywords: *SIS, MWCNT, rheological percolation, electrical percolation, self-assembly.*

How to cite: Ferreira, L. B., Fernandes, R. S., Bretas, R. E. S., & Santos, J. P. F. (2020). Melt-mixed nanocomposites of SIS/MWCNT: rheological, electrical and structural behavior. *Polímeros: Ciência e Tecnologia, 30*(4), e2020043. https://doi.org/10.1590/0104-1428.08220

1. Introduction

The use of multiwall carbon nanotubes (MWCNT) in polymeric matrixes to produce conductive nanocomposites has been widely studied[1,2]. Among the broad range of polymer matrixes, the thermoplastic elastomers have the advantage of behaving as elastomers at room temperature, but being able to be processed as thermoplastics[3]. Their elastomeric properties make them good candidates for proton exchange membranes[4], sensors[5,6], photoactuators[7], among others.

Thermoplastic elastomers based on block copolymers have an additional advantage: their morphologies are based on rigid domains that anchor flexible or elastomeric domains. The insertion of nanoparticles inside these domains constitutes one of the current approaches to produce nanocomposites for energy conversion and storage[8-10]; thus, due to the large variety of morphologies that these domains can assume, a myriad of possibilities exists. In a previous work of ours[3], flexible conductive nanocomposites based on the thermoplastic elastomer polystyrene-b-polybutadiene-b-polystyrene (SBS) filled with MWCNT were produced by solution casting followed by annealing during several days. These nanocomposites had a microstructure composed of hexagonally packed cylinders (HEX) co-existing with lamellar morphologies.

The triblock copolymer polystyrene-b-polyisoprene-b-polystyrene (SIS) belongs to the styrene based thermoplastics elastomers group and like SBS is extremely flexible and easily processable. SIS has a biphasic morphology, in which the polystyrene (PS) microdomains are dispersed through a flexible elastomeric matrix of polyisoprene (PI). Its flexible PI segments allow large deformations, while the PS domains act as physical cross-links anchoring the PI blocks, yielding an elastomeric response to the whole material[11,12]. Ilčíková et al.[7] produced nanocomposites of SIS filled with MWCNT by solution mixing. These authors found that these nanocomposites had photo-actuation abilities. Garate et al.[13] also produced nanocomposites of SIS/MWCNT by solution mixing. They improved the dispersion of the MWCNT into the SIS by grafting MWCNT with PS oligomers and using a surfactant. Brook et al.[14] produced conductive hybrid nanocomposites of SIS/MWCNT/Polyaniline (Pani) with improved thermal, mechanical and electrical properties. Ponnamma et al.[15] developed flexible oil sensors based on SIS/MWCNT nanocomposites. The materials showed best oil sensing abilities above the percolation level.

All the studies above cited used solution casting or solution precipitation as the processing method to obtain the SIS/MWCNT nanocomposites. However, it is known that

melt mixing is the most common method of compounding in the thermoplastic industry. Melt mixing is scalable for large productions, being also environmental friendly as it does not use toxic solvents and it is free of carbon emissions. Nevertheless, we were able to find only one study on melt mixing of SIS/MWCNT[16] and none on the analysis of the influence of MWCNT on the structure, relaxation and electrical properties of SIS after melt mixing.

Thus, in this work, nanocomposites with different volumetric fractions of MWCNT in SIS triblock copolymer were produced by melt mixing. To the best of our knowledge, this is the first work directed to perform a comprehensive study on the rheological, electrical and structural behavior of SIS/MWCNT nanocomposites produced by melt mixing.

2. Materials and Methods

2.1 Materials

The SIS triblock copolymer was donated by Kraton South America (Kraton D1162P) with 43 m.% of polystyrene (PS), antioxidant content between 0.08 and 0.30 m.%, density of 0.92 g/cm^3 and MFI of 45 g/10min, according to the manufacturer; the molar mass was not informed. The SIS was ground in a mill (Micron Powder Systems, model CF Bantam) at 100 rpm with injection of liquid nitrogen in order to obtain a micronized powder. Multiwall carbon nanotubes (MWCNTs), grade number NC7000, were supplied by Nanocyl S.A. with 90% purity. The MWCNT were characterized in earlier works of ours[3,17] by transmission electron microscopy (TEM) using a FEI TECNAI G F20 HRTEM at 80 kV and Raman spectroscopy using a Renishaw spectrometer, with in via Raman microscope, NIR laser, in the regular mode. By TEM, their external diameters (d=9.5 nm) and their average lengths (l=1.5 μm) were measured. By Raman spectroscopy, the peaks at 1355 and 1594 cm^{-1} attributed to the characteristics D and G bands of the MWCNT, respectively, were observed. The D band can be correlated to structural defects of the nanotubes, while the G band to *in plane* vibration of a sp^2 bonded structure. The D and G intensities ratio (I_D/I_G) is used as an indicator of the degree of imperfections of the carbon nanotube; the higher, the more defectives are the MWCNT. Another band at 2781 cm^{-1}, the G_o band, is correlated to the electronic properties of the carbon nanotube; thus, the ratio of the G_o and G intensities (I_{Go}/I_G) is used as an indicator of the metallicity of the carbon nanotube. The higher, the more metallic are the nanotubes. The calculated ratios were I_D/I_G =1.14 and I_{Go}/I_G=0.42[3], which indicated that the MWCNT were highly defectives and had a low metallicity[18]. White et al.[19] also found that the NC7000 Nanocyl grade had Al, Fe and Co as impurities and O on the surface.

Toluene (PA Synth) was used as a solvent.

2.2 Melt mixing

Prior to the processing, SIS and MWCNT were dried for 12 hours at 60 ºC. First, a masterbatch of 5 vol.% of MWCNT and SIS was produced using a torque rheometer Haake, model Rheomix 600p, at 190ºC, 100rpm, during 5 min. The masterbatch was then diluted with SIS to yield the final concentrations of MWCNT in the nanocomposites in the same Haake torque rheometer. The following MWCNT concentrations were used for this study: 0.1, 1.0, 3.0 and 5.0 vol.% MWCNT. These filler loadings were selected based on previous works[1,20,21], which pointed out a value of 0.31vol.% MWCNT for the theoretical percolation threshold of a generic polymer matrix filled with the MWCNT NC7000 from Nanocyl[1,3,22]. After melt mixing, films of the resulting nanocomposites were produced by compression molding at 190ºC under 8 MPa of pressure using a hot press. The samples were named SIS/MWCNT$_x$, where x represents the volumetric fraction of MWCNT.

As a benchmark, samples of neat SIS were produced by solvent casting to observe their quasi-equilibrium morphologies. First, the SIS powder was melted and later dissolved in toluene (concentration: 0.2 g/ml) under magnetic stirring for 2 h at 100ºC. The resulting solution was poured in Petri dishes to obtain films, which were maintained at room temperature during 4 h and then left in a vacuum oven at 110 ºC during eight days to enable the self-organization of SIS into well-ordered rigid and soft domains. This approach of annealing was done based on previous works[3,23,24].

Samples of the SIS/MWCNT nanocomposites were not prepared by solution, because as already reported in early work of ours on SBS/MWCNT nanocomposites[3] to allow complete solvent evaporation and to obtain self-standing films the casting process takes approximately 7 days to be completed.

2.3 Characterization

The rheological behavior of the nanocomposites was evaluated using a stress-controlled rheometer AR-G2, from TA Instruments, with parallel plates, diameter of 25 mm, gap of 1 mm between the plates, frequencies ω between 0.1 and 100 rad/s, at a temperature of 190 ºC. The complex viscosity $\eta^*(\omega) = \eta'(\omega) - i\eta''(\omega)$, where η' = dynamic viscosity and η'' = imaginary viscosity was obtained. The measurements were done within the linear viscoelastic regime. The electrical resistivity measurements of the nanocomposites were made using two setups. For samples with resistivity lower than 10^3 Ωm, two probe measurements were done using a stabilized source-meter device (Keithley, model 237) and parallel Pt electrodes having 1 cm diameter; for samples with electrical resistivity higher than 10^3 Ωm, a Keithley 6517A electrometer was used.

The domains structure of SIS was characterized by small angle x-rays scattering (SAXS) using an equipment from Bruker (AXS 2D Nanostar, Cu, Kα radiation, 30 mA, 40 kV), at scanning angles below 5º. The morphology of the nanocomposites was analyzed by transmission electron microscopy (TEM) and atomic force microscopy (AFM). TEM was done using an equipment from FEI company (Magellan 400L) at 20kV. AFM was done using an equipment from Veeco Digital Instruments, model MMA FM-2, with silicon cantilevers.

3. Results and Discussions

3.1 Rheological behavior

Figure 1 shows the complex viscosity as a function of frequency of the samples. The neat SIS and the SIS/MWCNT

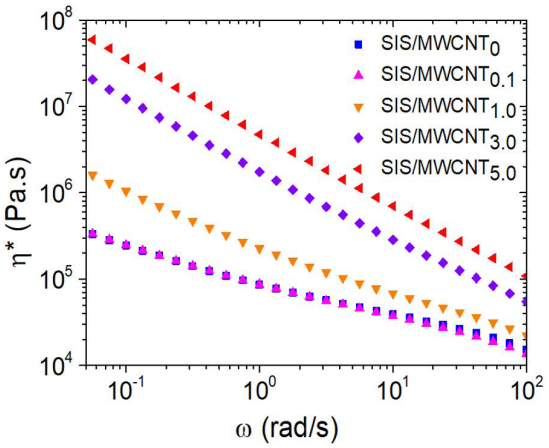

Figure 1. Complex viscosity (η*) versus oscillatory frequency (ω) of the nanocomposites.

nanocomposites showed a shear-thinning behavior; if a power law model ($\eta^* = m\omega^{n-1}$, where m=consistency and n=power law index) is fitted to the curves, a highly pseudoplastic behavior is observed (n→0). The nanocomposites containing higher amounts of MWCNT had higher η* than the others. It is known that MWCNT have high aspect ratios and high modulus. Therefore, the MWCNT can easily form entangled and rigid networks with the polymer macromolecules, unable to relax along the flow direction, thus increasing the flow resistance of the nanocomposites. Accordingly, the higher the MWCNT content the more entangled are these networks, yielding high viscosities in the molten state[25,26].

As said before, the complex viscosity has two components: η' and η". η' is proportional to the viscous response or energy dissipation of the material, while η" is proportional to the elastic response or energy storage. Therefore, the relationships between these viscosities and the components of the complex modulus $G^*(\omega) = G' + iG''$ are: $\eta' = G''/\omega$ and $\eta'' = G'/\omega$, where G" is the loss modulus and G' is the storage modulus. Figure 2 shows plots of η' and η" versus ω. It can be noted that, at lower MWCNT loadings, the viscous response is more pronounced than the elastic response; however, between 1-3vol.% MWCNT the elastic response became more pronounced than the viscous response through the broadband frequency range. That is, a transition from a predominantly liquid or viscous behavior to predominantly elastic or solid behavior occurred above 1 vol.% of MWCNT; i.e, the rheological percolation threshold was achieved.

Another way to obtain the value of the rheological percolation threshold is to use the slopes of the G'(ω) and G"(ω) curves at the terminal zone of the viscoelastic spectrum. It is worthwhile to recall that at the terminal zone, the frequencies are small; because the mechanical response of the macromolecules will be dependent on their relaxation times t_r $(\omega = 1/t_r)$, at the terminal zone, the responses will be associated to the parts of the macromolecules which have long relaxation times (mainly their backbones)[27-29]. A linear polymer of high molecular weight has *entanglement and disentanglement* of their coils[28,29], with the formation of a temporary network structure due to inter and intra-molecular junctions derived from the twisting and bending of the coils. Between these junctions (which are continually being formed and undone), the resistance to conformational changes will be low, and the elastic response, which is dependent upon the life time of these junctions will decay rapidly with the frequency, due to the macromolecules relaxation. The viscous response (which will reflect the flow resistance and energy dissipation) will also decay, but with less intensity. All the macromolecular models predict, therefore, that, at the terminal zone, $G' \sim \omega^2$ and $G'' \sim \omega$; that is, the slope of the $G'(\omega)$ curve at the terminal zone will be approximately 2 while the slope of the $G''(\omega)$ curve will be 1[28]. On the other hand, in a slightly crosslinked polymer, the junctions are permanent; therefore, the conformational changes between the crosslinks will be restrained and G' → G_e= equilibrium modulus, while G" will flatten. That is, both G' and G" will be independent of ω; therefore, if the slopes of the components of the complex modulus change towards zero at the terminal zone, a very restrained structure (a so called pseudo-solid behavior) will be attained. The change of slopes can, therefore, predicts the formation of a percolated network of MWCNT within the polymer, as others works have already shown[27,30-32].

The slopes at the terminal zone were calculated and are shown in Table 1.

The slopes of the $G'(\omega)$ and $G''(\omega)$ curves of the pure SIS were low, not even close to 2 and 1, respectively; that is, SIS, being elastomeric and having rigid styrene domains anchoring the isoprene domains and thus acting as crosslinking, has already a quasi-solid behavior. However, when 1 vol.% of MWCNT were added to the SIS, both slopes changed drastically to almost 0, confirming the complex viscosity analysis, that above 1 vol%. MWCNT the rheological percolation occurred. From a rheological point of view, at MWCNT loadings above the percolation threshold, an entangled and well-established network between SIS backbones and MWCNT exists.

From the crossover frequency ω_c (where G'=G"), the relaxation time at the beginning of the plateau region ($t_{r,c}$) and consequently the influence of the MWCNT on the SIS relaxation can be analyzed[27]. Table 1 shows also these values. The relaxation time of the SIS macromolecules is around 0.018 s; when 0.1 vol.% of MWCNT was added, the relaxation of the SIS macromolecules increased to 0.025 s while another (very high) relaxation time at 10 s surged due to the presence of the MWCNT. That is, some SIS macromolecules were restrained by the MWCNT, but the MWCNT themselves did not form a percolated network with the SIS macromolecules (MWCNT high relaxation time). However, when 1.0 vol.% of MWCNT is added, only one relaxation time at 0.13 s is observed, due to the formation of a restrained and percolated network. This result confirms the viscosity results, that is, the percolation concentration for the SIS/MWCNT was around 1 vol.% MWCNT.

3.2 Electrical behavior

The theory of electrical percolation predicts the dependence of electrical resistivity (ρ) versus filler volumetric loading (V) according to Equation 1 [33]:

$$\rho(V) \propto (V - V_c)^{-t} \text{ , when } V > Vc \quad (1)$$

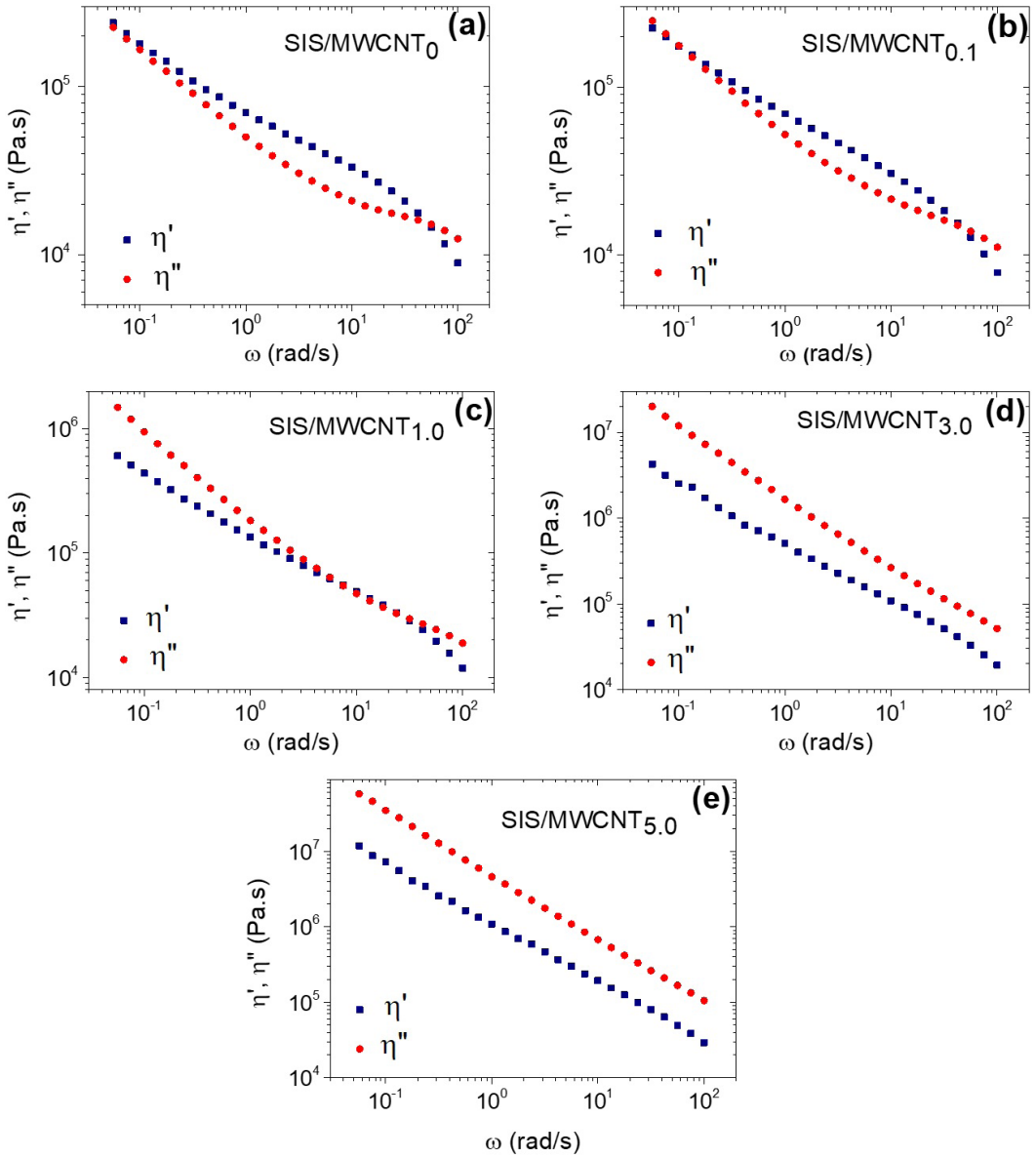

Figure 2. Real viscosity (η') and imaginary viscosity (η") versus oscillatory frequency (ω).

Table 1. Slopes (α) of the $G'(\omega)$ and $G''(\omega)$ curves, crossover frequency (ω_c) and relaxation time at crossover frequency ($t_{r,c}$).

Sample	α G'	α G"	ω_c (rad/s)	$t_{r,c}$ (s)
$SIS/MWCNT_{0.0}$	0.89	0.32	55	0.018
$SIS/MWCNT_{0.1}$	0.92	0.30	40, 0.1	0.025,10
$SIS/MWCNT_{1.0}$	0.19	0.02	7.5	0.13
$SIS/MWCNT_{3.0}$	0.01	0.01	-	-
$SIS/MWCNT_{5.0}$	0.01	0.02	-	-

Table 2. Electrical resistivity of the samples.

Sample	Resistivity (Ω.m)	Sample	Resistivity (Ω.m)
$SIS/MWCNT_{0.0}$	$1.2x10^{11}$	$SIS/MWCNT_{3.0}$	$1.7x10^{1}$
$SIS/MWCNT_{0.1}$	$1.2x10^{11}$	$SIS/MWCNT_{5.0}$	$1.5x10^{0}$
$SIS/MWCNT_{1.0}$	$4.4x10^{5}$		

where *Vc* is the electrical percolation threshold concentration and t is denominated critical exponent. Figure 3 shows a graph of electrical resistivity versus filler volumetric loading and Table 2 summarize these values. It can be observed that the electrical resistivity decreased various orders of magnitude with increasing MWCNT loading. By definition[3] at the electrical percolation concentration, the electrical conductivity increases promptly several orders of magnitude; however, in our case, there was a gradual increase of the conductivity (or decrease in resistivity), between 0.1 and 3 vol.% MWCNT. As the percolation-dispersion staircase model[34,35] has pointed out, when an abrupt increase of the conductivity occurs, only one conductivity mechanism exists, while if a gradual increase occurs, then multiple local conductivity mechanisms are contributing to the global conductivity. This latter behavior seems to predominate in the SIS/MWCNT

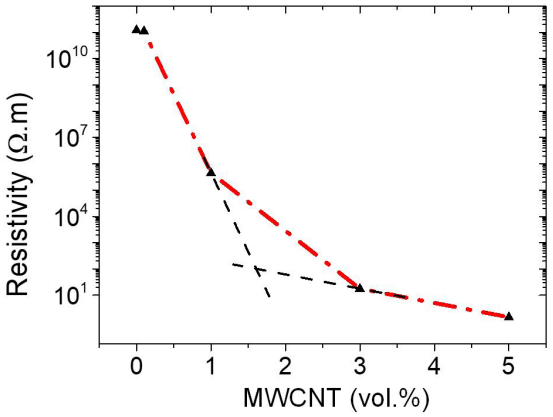

Figure 3. Volumetric resistivity versus MWCNT loading.

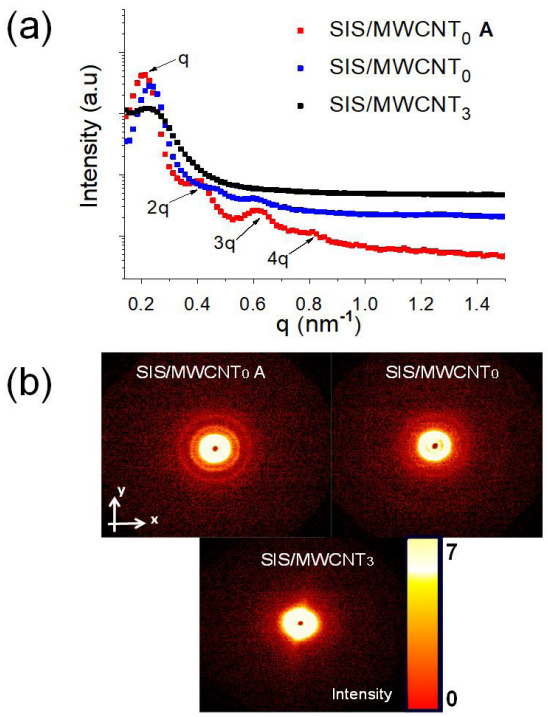

Figure 4. (a) Intensity I measured in SAXS experiments using compression molded films samples as a function of the magnitude q of the scattering vector (b) 2D SAXS patterns.

nanocomposites, as observed in other work of ours[3]. The multiple local conductivity mechanisms can be credited to the co-existence of different sizes of MWCNT aggregates with single MWCNT in the SIS matrix. Therefore, electrical conduction will occur through the aggregates, through the single MWCNT and through electron tunneling between adjacent MWCNT.

From Equation 1, *Vc*~1.6vol.% MWCNT and t~2.9. Thus, these melt mixed SIS/MWCNT nanocomposites percolated at MWCNT loadings significantly above the theoretical value (0.31vol.% MWCNT). In other works, solution prepared nanocomposites achieved the electrical percolation at lower MWCNT loadings[2,3,36]. Accordingly, to the statistical theory of percolation[37], a minimum amount of filler for electrical conduction in a nanocomposite[38] is required. This minimum amount is called the electrical percolation threshold. The fillers must touch each other or being close enough to allow the establishment of conduction paths for the charge carriers (electrons, holes or ions). Therefore, the higher the MWCNT loading the higher the probability of establishing these paths. As well, the higher the aspect ratio of the MWCNT, the higher the probability of the nanotubes to touch each other[18]. During melt mixing, however, a damage and breakage of the MWCNTs (or other rigid nanoparticles) due to the shear stresses can occur, as it has been observed in other works[30,39-41], Thus, for melt mixed nanocomposites, a shifting of the percolation threshold towards higher filler loadings compared with solution mixed nanocomposites[1,41] is expected.

The critical exponent t can be correlated with the system dimensionality and with conduction mechanisms. As pointed out by Bauhofer and Kovacs in their throughout review[2], values of t~3.0 were obtained using a Bethe lattice and Mean field theory. These theories correlated increasing values of t with conduction by tunneling effects. When the MWCNT-MWCNT distances are below 10 nm, the electrons can jump from one nanotube to another[42,43]. The higher the MWCNT loading, the shorter the distance between the MWCNT, thus increasing the chance of electrons to surpass the barrier. Probably, in these SIS/MWCNT nanocomposites there were individual and well-dispersed MWCNT coexisting with remaining MWCNT aggregates, as said before. By increasing the amount of MWCNT the individual MWCNT and MWCNT aggregates became closer enough to allow conduction by hopping and tunneling effects.

3.3 Structural characterization

SAXS profiles and 2D patterns of some of the samples are shown in Figure 4a and 4b, respectively. The scattering vector is $q=(4\pi/\lambda)sen\theta$, where λ is the wavelength and 2θ the scattering angle. As expected, the sample of pure SIS from annealing treatment (SIS/MWCNT$_0$ A) displayed concentric rings and SAXS peaks at q =0.2 nm^{-1}, 2q = 0.4 nm^{-1}, 3q=0.6 nm^{-1} and 4q = 0.8 nm^{-1}, which are ascribed to lamellar morphologies[3,44]. That is, eight days were enough time to allow the self-organization of SIS into well-ordered lamellar domains.

On the other hand, the sample of pure SIS produced by melt mixing (SIS/MWCNT$_0$) showed less evident peaks and hallo rings; in the sample SIS containing 3 vol% MWCMT (SIS/MWCNT$_3$), the peaks and hallo rings were absent. This result shows that both melt mixing and the presence of MWCNT hampered the self-assembly of SIS domains. Figure 5a depicts an AFM micrograph of the SIS/MWCNT$_0$ sample, where typical lamellar morphologies can be observed; the PS domains can be identified as the yellow ones (higher elastic moduli) while the PI domains are the brown (lower elastic moduli). PS and PI domains presented average thicknesses of 21.0 nm and 13.1 nm, respectively.

It is known that the stability of different equilibrium domain morphologies of a block copolymer depends on the relationship between enthalpy (interaction energies between dissimilar polymer blocks given by the Flory-Huggins interaction parameter, χ) and entropy (conformational energy

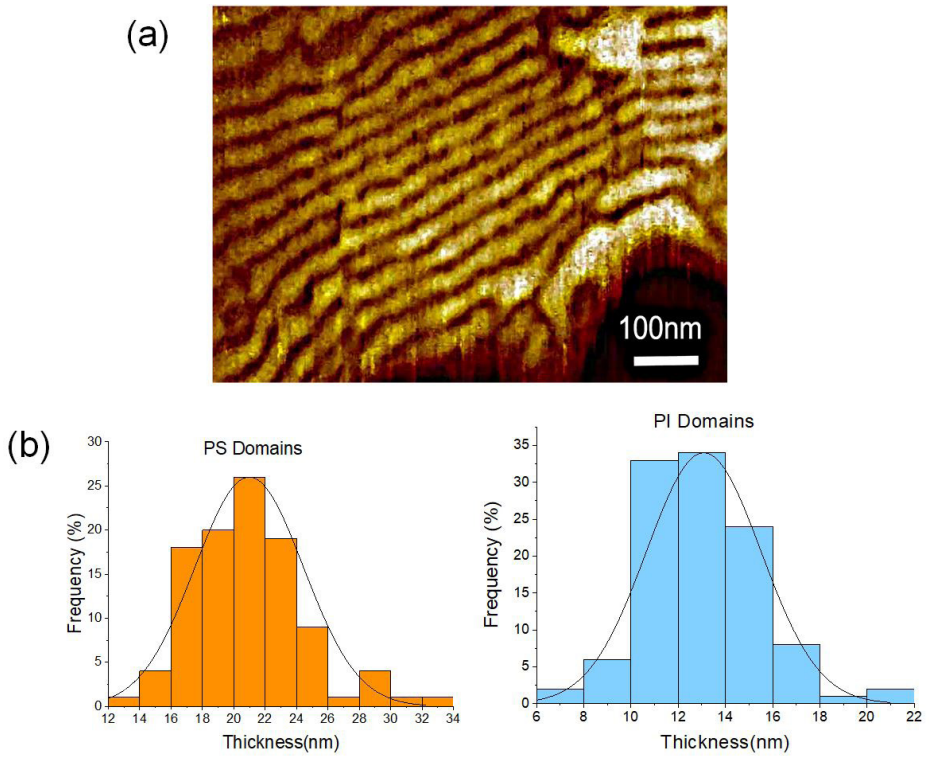

Figure 5. (a) AFM micrograph of SIS/MWCNT$_0$ A annealed during eight days; (b) Distributions of thickness of the lamellar PS and PI domains.

depending on the degree of polymerization, N). For di-blocks copolymers, it has been observed that when $\chi N > 10.5$ different stable and even co-existing morphologies can be obtained depending on the values of χN and f, the volumetric fraction of one of the co-monomers. Numerous studies have showed various types of equilibrium morphologies of di-blocks AB and tri-blocks ABA copolymers, which are spheres (S), cylinders (C), lamellas (L) and gyroids (G)[45-47]. When f is near 0.5, lamellar morphologies are usually expected after annealing during several days. In fact, the SIS employed in this work has a PS molar fraction ~43%, that is, f is near 0.5.

However, when $\chi N < 10.5$ only a disordered melt is formed[48]. In general, long times are required to self-assembly domains from the melt or solution; therefore, in the melt compounding process employed to prepare SIS/MWCNT nanocomposites probably time was not enough to allow the self-assembly of PS and PI into well-ordered domains. Moreover, it is known that even small changes in temperature or shearing can induce large changes in these equilibrium morphologies[49].

Figure 6a shows TEM micrographs of the MWCNT as received, prior to the mixing with SIS. Figure 6b shows a TEM micrograph of the nanocomposite containing 3 vol% MWCNT. This sample was selected because its MWCNT loading was above both, the rheological and electrical percolations. The MWCNT can be seen as long and entangled tubes through the SIS matrix. The measurement of the lengths of the MWCNT was difficult because they were highly entangled; however, comparison of the micrographs Figure 6a and Figure 6b clearly suggests that a reduction of

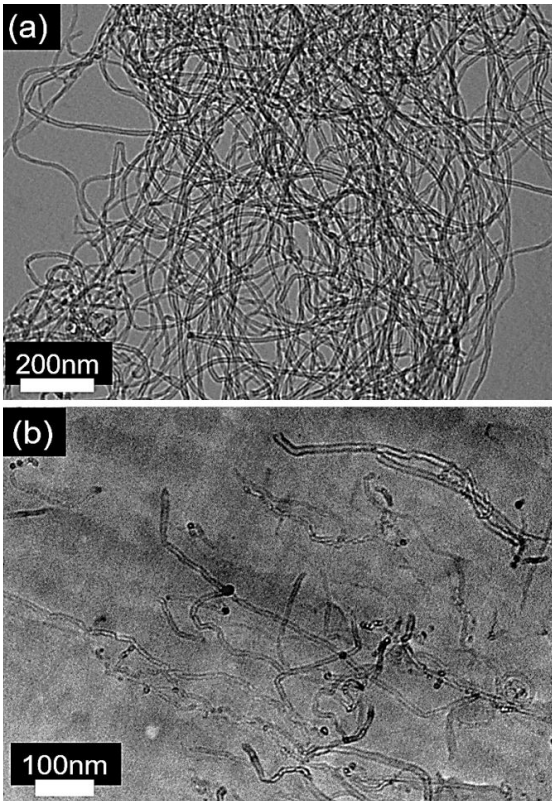

Figure 6. TEM images: (a) Pure MWCNT, (b) Nanocomposite SIS/ 3vol.% MWCNT.

the MWCNT lengths occurred during the process of melt mixing, as already pointed out in other works[1,50]. In addition, Figure 6b shows that the MWCNT touch each other and are close enough to allow the establishment of electrical conduction paths. As pointed out by SAXS measurements, there was a reduction of regularity of the SIS domains from the sample SIS/MWCNT$_0$ to the sample SIS/MWCNT$_3$, thus MWCNT hampered the self-assembly of SIS, which is in line with previous works[3,51]. The presence of MWCNT can change the correlation between enthalpy and entropy[10]; for example, π-π interactions can be established between the MWCNT graphitic structure, the phenyl groups from PS and the doubles bonds from the PI backbones[52,53]. Moreover, MWCNT are rigid structures having ultrahigh moduli[54], thus being physical barriers against molecular motion of the PS and PI blocks.

Other works have shown that modifying the surface of MWCNT can cause remarkable changes in the self-assembly of MWCNT/block copolymers composites. For example, grafting PS chains on MWCNT surfaces influenced the domains morphology of SBS/MWCNT composites[55]; instead of being inserted in the PS domains, the PS-g-MWCNT templates the lamellar PS domains morphology. Other studies have concluded that the MWCNT are inserted in both rigid and soft domains of SBS[56] or SIS[13].

4. Conclusions

Nanocomposites with different volumetric fractions of MWCNT in SIS block copolymers were produced by melt mixing. Both, rheological and electrical percolation thresholds were achieved at MWCNT loadings between 1-3 vol.%. The complex viscosity increased two orders of magnitude from neat SIS to SIS/5vol.%MWCNT, while electrical resistivity decreased eleven orders of magnitude from neat SIS to SIS/5vol.%MWCNT. Therefore, conductive nanocomposites were obtained. Moreover, the presence of MWCNT significantly enhanced the relaxation of SIS blocks. Structural characterization revealed that both, the melt mixing process and the presence of MWCNT hampered the self-assembly of SIS into well-ordered domains.

5. Acknowledgements

The authors are grateful to Programa de Educação Tutorial em Engenharia de Materiais (PET) of Centro Federal de Educação Tecnológica de Minas Gerais (CEFET-MG), to Fundação de Amparo à Pesquisa do Estado de São Paulo - FAPESP (2013/07296-2, 2013/03118-2, 2014/17597-2, 2016/03667-4) and Conselho Nacional de Desenvolvimento Científico e Tecnológico - CNPQ (573636/2008-7, 141456/2013-2 and 10086/2019) for the financial support, to Kraton for the SIS donation, to Prof. Marcelo Orlandi (Unesp) for some of the electrical measurements and to Prof. Edson R. Leite, Ms. Renata Sala and Mr.William Leonel (LIEC-UFSCar) for the SAXS measurements.

6. References

1. Santos, J. P. F., de Melo Carvalho, B., & Suman Bretas, R. E. (2019). Remarkable change in the broadband electrical behavior of poly(vinylidene fluoride)–multiwalled carbon nanotube nanocomposites with the use of different processing routes. *Journal of Applied Polymer Science*, *136*(17), 1-10. http://dx.doi.org/10.1002/app.47409.
2. Bauhofer, W., & Kovacs, J. Z. (2009). A review and analysis of electrical percolation in carbon nanotube polymer composites. *Composites Science and Technology*, *69*(10), 1486-1498. http://dx.doi.org/10.1016/j.compscitech.2008.06.018.
3. Ferreira Santos, J. P., França Melo, G. H., Gonçalves, A. M., Eiras, J. A., & Suman Bretas, R. E. (2018). Flexible conductive poly(styrene-butadiene-styrene)/carbon nanotubes nanocomposites: self-assembly and broadband electrical behavior. *Journal of Applied Polymer Science*, *135*(34), e46650. http://dx.doi.org/10.1002/app.46650.
4. Kim, J., Kim, B., & Jung, B. (2002). Proton conductivities and methanol permeabilities of membranes made from partially sulfonated polystyrene-block-poly(ethylene-ran-butylene)-block-polystyrene copolymers. *Journal of Membrane Science*, *207*(1), 129-137. http://dx.doi.org/10.1016/S0376-7388(02)00138-2.
5. Ji, M., Deng, H., Yan, D., Li, X., Duan, L., & Fu, Q. (2014). Selective localization of multi-walled carbon nanotubes in thermoplastic elastomer blends: an effective method for tunable resistivity-strain sensing behavior. *Composites Science and Technology*, *92*, 16-26. http://dx.doi.org/10.1016/j.compscitech.2013.11.018.
6. Costa, P., Ribeiro, S., & Lanceros-Mendez, S. (2015). Mechanical vs. electrical hysteresis of carbon nanotube/styrene-butadiene-styrene composites and their influence in the electromechanical response. *Composites Science and Technology*, *109*, 1-5. http://dx.doi.org/10.1016/j.compscitech.2015.01.006.
7. Ilčíková, M., Mrlík, M., Sedláček, T., Chorvát, D., Krupa, I., Šlouf, M., Koynov, K., & Mosnáček, J. (2014). Viscoelastic and photo-actuation studies of composites based on polystyrene-grafted carbon nanotubes and styrene-b-isoprene-b-styrene block copolymer. *Polymer*, *55*(1), 211-218. http://dx.doi.org/10.1016/j.polymer.2013.11.031.
8. Hoheisel, T. N., Hur, K., & Wiesner, U. B. (2015). Block copolymer-nanoparticle hybrid self-assembly. *Progress in Polymer Science*, *40*, 3-32. http://dx.doi.org/10.1016/j.progpolymsci.2014.10.002.
9. Sarkar, B., & Alexandridis, P. (2014). Block copolymer-nanoparticle composites: Structure, functional properties, and processing. *Progress in Polymer Science*, *40*, 33-62. http://dx.doi.org/10.1016/j.progpolymsci.2014.10.009.
10. Chiu, J. J., Kim, B. J., Kramer, E. J., & Pine, D. J. (2005). Control of nanoparticle location in block copolymers. *Journal of the American Chemical Society*, *127*(14), 5036-5037. http://dx.doi.org/10.1021/ja050376i. PMid:15810835.
11. Silva, S. A., Marques, C. L., & Cardozo, N. S. M. (2012). Composition and performance of styrene-isoprene-styrene (SIS) and styrene-butadiene-styrene (SBS) hot melt pressure sensitive adhesives. *The Journal of Adhesion*, *88*(2), 187-199. http://dx.doi.org/10.1080/00218464.2012.648873.
12. Phillips, J. P., Deng, X., Stephen, R. R., Fortenberry, E. L., Todd, M. L., McClusky, D. M., Stevenson, S., Misra, R., Morgan, S., & Long, T. E. (2007). Nano- and bulk-tack adhesive properties of stimuli-responsive, fullerene–polymer blends, containing polystyrene-block-polybutadiene-block-polystyrene and polystyrene-block-polyisoprene-block-polystyrene rubber-based adhesives. *Polymer*, *48*(23), 6773-6781. http://dx.doi.org/10.1016/j.polymer.2007.08.050.
13. Garate, H., Fascio, M. L., Mondragon, I., D'Accorso, N. B., & Goyanes, S. (2011). Surfactant-aided dispersion of polystyrene-functionalized carbon nanotubes in a nanostructured poly (styrene-b-isoprene-b-styrene) block copolymer. *Polymer*, *52*(10), 2214-2220. http://dx.doi.org/10.1016/j.polymer.2011.03.032.

14. Brook, I., Mechrez, G., Suckeveriene, R. Y., Tchoudakov, R., & Narkis, M. (2013). A novel approach for preparation of conductive hybrid elastomeric nano-composites. *Polymers for Advanced Technologies*, *24*(8), 758-763. http://dx.doi.org/10.1002/pat.3142.
15. Ponnamma, D., Sadasivuni, K. K., Thomas, S., Krupa, I., & AlMa'adeed, M. A.-A. (2016). Flexible oil sensors based on multiwalled carbon nanotube-filled isoprene elastomer composites. *Rubber Chemistry and Technology*, *89*(2), 306-315. http://dx.doi.org/10.5254/rct.15.84841.
16. Jo, Y., Kim, J. Y., Kim, S. Y., Seo, Y. H., Jang, K. S., Lee, S. Y., Jung, S., Ryu, B. H., Kim, H. S., Park, J. U., Choi, Y., & Jeong, S. (2017). 3D-printable, highly conductive hybrid composites employing chemically-reinforced, complex dimensional fillers and thermoplastic triblock copolymers. *Nanoscale*, *9*(16), 5072-5084. http://dx.doi.org/10.1039/C6NR09610G. PMid:28181617.
17. Santos, J. P. F., da Silva, A. B., Sundararaj, U., & Bretas, R. E. S. (2015). Novel electrical conductive hybrid nanostructures based on PA 6/MWCNTCOOH electrospun nanofibers and anchored MWCNTCOOH. *Polymer Engineering and Science*, *55*(6), 1263-1272. http://dx.doi.org/10.1002/pen.24064.
18. Cui, H., Eres, G., Howe, J. Y., Puretkzy, A., Varela, M., Geohegan, D. B., & Lowndes, D. H. (2003). Growth behavior of carbon nanotubes on multilayered metal catalyst film in chemical vapor deposition. *Chemical Physics Letters*, *374*(3–4), 222-228. http://dx.doi.org/10.1016/S0009-2614(03)00701-2.
19. White, C. M., Banks, R., Hamerton, I., & Watts, J. F. (2016). Characterisation of commercially CVD grown multi-walled carbon nanotubes for paint applications. *Progress in Organic Coatings*, *90*, 44-53. http://dx.doi.org/10.1016/j.porgcoat.2015.09.020.
20. Chiu, F. C. (2014). Comparisons of phase morphology and physical properties of PVDF nanocomposites filled with organoclay and/or multi-walled carbon nanotubes. *Materials Chemistry and Physics*, *143*(2), 681-692. http://dx.doi.org/10.1016/j.matchemphys.2013.09.054.
21. Celzard, A., McRae, E., Deleuze, C., Dufort, M., Furdin, G., & Marêché, J. F. (1996). Critical concentration in percolating systems containing a high-aspect-ratio filler. *Physical review. B, Condensed matter*, *53*(10), 6209-6214. http://dx.doi.org/10.1103/PhysRevB.53.6209. PMid:9982020.
22. White, C. M., Banks, R., Hamerton, I., & Watts, J. F. (2016). Characterisation of commercially CVD grown multi-walled carbon nanotubes for paint applications. *Progress in Organic Coatings*, *90*, 44-53. http://dx.doi.org/10.1016/j.porgcoat.2015.09.020.
23. Georgopanos, P., Handge, U. A., Abetz, C., & Abetz, V. (2016). Influence of block sequence and molecular weight on morphological, rheological and dielectric properties of weakly and strongly segregated styrene-isoprene triblock copolymers. *Polymer*, *104*, 279-295. http://dx.doi.org/10.1016/j.polymer.2016.02.039.
24. Sakamoto, N., Hashimoto, T., Han, C. D., Kim, D., & Vaidya, N. Y. (1997). Order−order and order−disorder transitions in a polystyrene-block-polyisoprene-block-polystyrene copolymer. *Macromolecules*, *30*(6), 1621-1632. http://dx.doi.org/10.1021/ma960610c.
25. Ecco, L. G., Dul, S., Schmitz, D. P., Barra, G. M. O., Soares, B. G., Fambri, L., & Pegoretti, A. (2018). Rapid prototyping of efficient electromagnetic interference shielding polymer composites via fused deposition modeling. *Applied Sciences (Switzerland)*, *9*(1), 37-56. http://dx.doi.org/10.3390/app9010037.
26. Hoseini, M., Haghtalab, A., & Famili, M. H. N. (2017). Rheology and morphology study of immiscible linear low-density polyethylene/poly(lactic acid) blends filled with nanosilica particles. *Journal of Applied Polymer Science*, *134*(46), 1-12. http://dx.doi.org/10.1002/app.45526.
27. Beatrice, C. A. G., Branciforti, M. C., Alves, R. M. V., & Bretas, R. E. S. (2010). Rheological, mechanical, optical, and transport properties of blown films of polyamide 6/residual monomer/montmorillonite nanocomposites. *Journal of Applied Polymer Science*, *116*(6), 3581-3592. http://dx.doi.org/10.1002/app.31898.
28. Bueche, F. (1970). Viscoelastic properties of polymers. *Polymer Letters*, *8*(8), 595. http://dx.doi.org/10.1002/pol.1970.110080815.
29. Edwards, S. (1988). Dynamics of polymeric liquids. *British Polymer Journal*, *20*(3), 299-302. http://dx.doi.org/10.1002/pi.4980200323.
30. Marini, J., & Bretas, R. E. S. (2013). Influence of shape and surface modification of nanoparticle on the rheological and dynamic-mechanical properties of polyamide 6 nanocomposites. *Polymer Engineering and Science*, *53*(7), 1512-1528. http://dx.doi.org/10.1002/pen.23405.
31. Zhao, J., Morgan, A. B., & Harris, J. D. (2005). Rheological characterization of polystyrene-clay nanocomposites to compare the degree of exfoliation and dispersion. *Polymer*, *46*(20), 8641-8660. http://dx.doi.org/10.1016/j.polymer.2005.04.038.
32. Marini, J., & Bretas, R. E. S. (2013). Influence of shape and surface modification of nanoparticle on the rheological and dynamic-mechanical properties of polyamide 6 nanocomposites. *Polymer Engineering and Science*, *53*(7), 1512-1528. http://dx.doi.org/10.1002/pen.23405.
33. Arjmand, M., Mahmoodi, M., Gelves, G. A., Park, S., & Sundararaj, U. (2011). Electrical and electromagnetic interference shielding properties of flow-induced oriented carbon nanotubes in polycarbonate. *Carbon*, *49*(11), 3430-3440. http://dx.doi.org/10.1016/j.carbon.2011.04.039.
34. Balberg, I., Azulay, D., Goldstein, Y., Jedrzejewski, J., Ravid, G., & Savir, E. (2013). The percolation staircase model and its manifestation in composite materials. *European Physical Journal*, *86*(10), 428-445. http://dx.doi.org/10.1140/epjb/e2013-40200-7.
35. Pötschke, P., Dudkin, S. M., & Alig, I. (2003). Dielectric spectroscopy on melt processed polycarbonate: multiwalled carbon nanotube composites. *Polymer*, *44*(17), 5023-5030. http://dx.doi.org/10.1016/S0032-3861(03)00451-8.
36. Santos, J. P. F., Arjmand, M., Melo, G. H. F., Chizari, K., Bretas, R. E. S., & Sundararaj, U. (2018). Electrical conductivity of electrospun nanofiber mats of polyamide 6/polyaniline coated with nitrogen-doped carbon nanotubes. *Materials & Design*, *141*, 333-341. http://dx.doi.org/10.1016/j.matdes.2017.12.052.
37. Berhan, L., & Sastry, A. M. (2007). Modeling percolation in high-aspect-ratio fiber systems. I. Soft-core versus hard-core models. *Physical Review E: Covering Statistical, Nonlinear, and Soft Matter Physics*, *75*(4), 1-8. http://dx.doi.org/10.1103/PhysRevE.75.041120. PMid:17500878.
38. Nasti, G., Gentile, G., Cerruti, P., Carfagna, C., & Ambrogi, V. (2016). Double percolation of multiwalled carbon nanotubes in polystyrene/polylactic acid blends. *Polymer*, *99*, 193-203. http://dx.doi.org/10.1016/j.polymer.2016.06.058.
39. Calisi, N., Giuliani, A., Alderighi, M., Schnorr, J. M., Swager, T. M., Di Francesco, F., & Pucci, A. (2013). Factors affecting the dispersion of MWCNTs in electrically conducting SEBS nanocomposites. *European Polymer Journal*, *49*(6), 1471-1478. http://dx.doi.org/10.1016/j.eurpolymj.2013.03.029.
40. Fu, S. Y., Chen, Z. K., Hong, S., & Han, C. C. (2009). The reduction of carbon nanotubes (CNT) length during the manufacturing of CNT/polymer composites and a method to simultaneously determine the resulting CNT and interfacial strenghts. *Carbon*, *47*(14), 3192-3200. http://dx.doi.org/10.1016/j.carbon.2009.07.028.
41. Kuester, S., Barra, G. M. O., Ferreira, J. C., Jr., Soares, B. G., & Demarquette, N. R. (2016). Electromagnetic interference shielding and electrical properties of nanocomposites based on poly (styrene-b-ethylene-ran-butylene-b-styrene) and carbon

nanotubes. *European Polymer Journal*, *77*, 43-53. http://dx.doi.org/10.1016/j.eurpolymj.2016.02.020.

42. Oskouyi, A. B., Sundararaj, U., & Mertiny, P. (2014). Tunneling conductivity and piezoresistivity of composites containing randomly dispersed conductive nano-platelets. *Materials (Basel)*, *7*(4), 2501-2521. http://dx.doi.org/10.3390/ma7042501. PMid:28788580.
43. Hu, N., Karube, Y., Yan, C., Masuda, Z., & Fukunaga, H. (2008). Tunneling effect in a polymer/carbon nanotube nanocomposite strain sensor. *Acta Materialia*, *56*(13), 2929-2936. http://dx.doi.org/10.1016/j.actamat.2008.02.030.
44. Shi, W., Li, W., Delaney, K. T., Fredrickson, G. H., Kramer, E. J., Ntaras, C., Avgeropoulos, A., & Lynd, N. A. (2016). Morphology re-entry in asymmetric PS-PI-PS' triblock copolymer and PS homopolymer blends. *Journal of Polymer Science. Part B, Polymer Physics*, *54*(2), 169-179. http://dx.doi.org/10.1002/polb.23811.
45. Lin, T. C., Yang, K. C., Georgopanos, P., Avgeropoulos, A., & Ho, R. M. (2017). Gyroid-structured nanoporous polymer monolith from PDMS-containing block copolymers for templated synthesis. *Polymer*, *126*, 360-367. http://dx.doi.org/10.1016/j.polymer.2017.04.045.
46. Lee, S., Lee, K., Jang, J., Choung, J. S., Choi, W. J., Kim, G. J., Kim, Y. W., & Shin, J. (2017). Sustainable poly(ε-decalactone)–poly(L-lactide) multiarm star copolymer architectures for thermoplastic elastomers with fixed molar mass and block ratio. *Polymer*, *112*, 306-317. http://dx.doi.org/10.1016/j.polymer.2017.02.008.
47. Sota, N., Saijo, K., Hasegawa, H., Hashimoto, T., Amemiya, Y., & Ito, K. (2013). Directed self-assembly of block copolymers into twin BCC-sphere: phase transition process from aligned hex-cylinder to BCC-sphere induced by a temperature jump between the two equilibrium phases. *Macromolecules*, *46*(6), 2298-2316. http://dx.doi.org/10.1021/ma400039p.
48. Stadler, R., Auschra, C., Beckmann, J., Krappe, U., Voight-Martin, I., & Leibler, L. (1995). Morphology and thermodynamics of symmetric poly (A-block-B-block-C) triblock copolymers. *Macromolecules*, *28*(9), 3080-3091. http://dx.doi.org/10.1021/ma00113a010.
49. Mishra, V., Fredrickson, G. H., & Kramer, E. J. (2011). SCFT simulations of an order–order transition in thin films of diblock and triblock copolymers. *Macromolecules*, *44*(13), 5473-5480. http://dx.doi.org/10.1021/ma200297f.
50. Chen, G. X., Li, Y., & Shimizu, H. (2007). Ultrahigh-shear processing for the preparation of polymer/carbon nanotube composites. *Carbon*, *45*(12), 2334-2340. http://dx.doi.org/10.1016/j.carbon.2007.07.017.
51. Li, Y., & Shimizu, H. (2009). Toward a stretchable, elastic, and electrically conductive nanocomposite: morphology and properties of poly[styrene-b-(ethylene-co-butylene)-b-styrene]/multiwalled carbon nanotube composites fabricated by high-shear processing. *Macromolecules*, *42*(7), 2587-2593. http://dx.doi.org/10.1021/ma802662c.
52. Tournus, F., Latil, S., Heggie, M. I., & Charlier, J.-C. (2005). π-stacking interaction between carbon nanotubes and organic molecules. *Physical Review. B*, *72*(7), 1-5. http://dx.doi.org/10.1103/PhysRevB.72.075431.
53. Lu, L., Zhou, Z., Zhang, Y., Wang, S., & Zhang, Y. (2007). Reinforcement of styrene–butadiene–styrene tri-block copolymer by multi-walled carbon nanotubes via melt mixing. *Carbon*, *45*(13), 2621-2627. http://dx.doi.org/10.1016/j.carbon.2007.08.025.
54. Kaseem, M., Hamad, K., & Ko, Y. G. (2016). Fabrication and materials properties of polystyrene/carbon nanotube (PS/CNT) composites: a review. *European Polymer Journal*, *79*, 36-62. http://dx.doi.org/10.1016/j.eurpolymj.2016.04.011.
55. Albuerne, J., Fierro, A. B., Abetz, C., Fierro, D., & Abetz, V. (2011). Block copolymer nanocomposites based on multiwall carbon nanotubes: effect of the functionalization of multiwall carbon nanotubes on the morphology of the block copolymer. *Advanced Engineering Materials*, *13*(8), 803-810. http://dx.doi.org/10.1002/adem.201000291.
56. Inukai, S., Niihara, K., Noguchi, T., Ueki, H., Magario, A., Yamada, E., Inagaki, S., & Endo, M. (2011). Preparation and properties of multiwall carbon nanotubes/ polystyrene-block-polybutadiene-block-polystyrene composites. *Industrial & Engineering Chemistry Research*, *50*(13), 8016-8022. http://dx.doi.org/10.1021/ie102380t.

Received: Aug. 30, 2020
Revised: Jan. 11, 2021
Accepted: Feb. 02, 2021